

# Ordering of the Heisenberg spin glass in high dimensions

Daisuke Imagawa\* and Hikaru Kawamura†

*Graduate School of Science, Osaka University, Toyonaka, Osaka 560-0043, Japan*

(Dated: February 1, 2008)

Ordering of the Heisenberg spin glass with the nearest-neighbor Gaussian coupling is investigated by equilibrium Monte Carlo simulations in four and five dimensions. Ordering of the mean-field Heisenberg spin glass is also studied for comparison. Particular attention is paid to the nature of the spin-glass and chiral-glass orderings. Our numerical data suggest that, in five dimensions, the model exhibits a single spin-glass transition at a finite temperature, where the spin-glass order accompanying the simultaneous chiral-glass order sets in. In four dimensions, the model exhibits a marginal behavior. Chiral-glass transition at a finite temperature not accompanying the standard spin-glass order is likely to occur, while the critical region associated with the chiral-glass transition is very narrow suggesting that the dimension four is close to the marginal dimensionality.

## I. INTRODUCTION

In numerical studies of spin glasses (SGs), much effort has been devoted to clarify the properties of the so-called Edwards-Anderson (EA) model<sup>1</sup>. Most of these numerical works on the EA model have concentrated on the Ising EA model. It is also very important, however, to clarify the properties of the corresponding Heisenberg model. This is simply due to the fact that many of real SG magnets are Heisenberg-like rather than Ising-like in the sense that the magnetic anisotropy is considerably weaker than the isotropic exchange interaction.<sup>1,2</sup>

Indeed, several numerical works have been performed on the Heisenberg EA model. Earlier numerical studies suggested that, in apparent contrast to experiments, the isotropic Heisenberg SG in three dimensions (3D) did not exhibit an equilibrium SG transition at any finite temperature.<sup>2,3,4,5,6,7,8</sup> This observation leads to general belief that the weak random magnetic anisotropy is crucially important in realizing a finite-temperature SG transition and a stable SG phase, which causes a crossover from the  $T_g = 0$  isotropic Heisenberg behavior to the  $T_g > 0$  anisotropic Ising behavior. The expected Heisenberg-to-Ising crossover, however, has not been observed experimentally, and this puzzle has remained unexplained.<sup>1,2</sup>

Meanwhile, a novel possibility was suggested by one of the present authors (H.K.) that the 3D Heisenberg SG might exhibit an equilibrium phase transition at a finite temperature, not in the spin sector as usually envisaged, but in the chirality sector, i.e., might exhibit a chiral-glass transition.<sup>6</sup> Chirality is a multispin variable representing the sense or the handedness of local noncoplanar spin structures induced by spin frustration. In the chiral-glass ordered state, the chirality is ordered in a spatially random manner while the Heisenberg spin remains paramagnetic. References<sup>6,8,9,10,11,12</sup> claimed that the standard SG order associated with the freezing of the Heisenberg spin occurred at a temperature lower than the chiral-glass transition temperature at  $T = T_{\text{SG}} < T_{\text{CG}}$ , quite possibly  $T_{\text{SG}} = 0$ . It means that the spin and the chirality are decoupled on long length scales (spin-chirality decoupling). In fact, based on such a spin-chirality decoupling picture, a chirality scenario of the SG transition has been advanced, which explains the experimentally observed SG transition as essentially chirality driven<sup>6,9</sup>. Note that the numerical observation of a finite-temperature chiral-glass transition in the 3D Heisenberg SG of Refs.<sup>6,8,9,10,11,12</sup> is not inconsistent with the earlier observations of the absence of the conventional SG order at any finite temperature.

Recently, however, in a series of numerical studies on the 3D Heisenberg EA model, Tohoku group criticized the earlier numerical works, claiming that in the 3D Heisenberg SG the spin ordered at a finite temperature and that the SG transition temperature might coincide with the chiral-glass transition temperature, i.e.,  $T_{\text{SG}} = T_{\text{CG}} > 0$ <sup>13,14</sup>. By contrast, Hukushima and Kawamura maintained that in 3D the spin and the chirality were decoupled on sufficiently long length scales, and that  $T_{\text{SG}} < T_{\text{CG}}$ <sup>15</sup>, supporting the earlier numerical results. The situation in 3D thus remains controversial.

Under such circumstances, in order to shed further light on the nature of the ordering in 3D, it might be useful to study the problem for the general space dimensionality  $D$ , particularly for dimensions higher than  $D = 3$ . In the limit of infinite dimensions  $D \rightarrow \infty$ , the model reduces to the corresponding mean-field model, i.e., the Heisenberg Sherrington-Kirkpatrick (SK) model. In the case of equal weights of the ferromagnetic and antiferromagnetic interactions, the SK model is known to exhibit a single continuous SG transition. Hence, in the  $D \rightarrow \infty$  limit, the order parameter of the transition is the Heisenberg spin itself, with no exotic phase such as the chiral-glass phase. Furthermore, the SG ordered state of the SK model is known to exhibit a hierarchical type of replica-symmetry breaking (RSB), i.e., a full RSB.

Then, questions which naturally arise are: (i) What is the lower critical dimension (LCD) of the SG order  $d_\ell^{\text{SG}}$ ? (ii) Is  $d_\ell^{\text{SG}}$  the same as the LCD associated with the chiral-glass order  $d_\ell^{\text{CG}}$ ?

Concerning the point (i), several earlier numerical studies including the high-temperature expansion<sup>16</sup> and the numerical domain-wall renormalization-group calculation<sup>4,17</sup> suggested that  $d_\ell^{\text{SG}}$  might be close to four. Meanwhile, Anderson and Pond argued that  $d_\ell^{\text{SG}} = 3$ <sup>18</sup>. First Monte Carlo (MC) simulation on the high-dimensional Heisenberg EA model was performed by Stauffer and Binder<sup>19</sup>. By studying the temporal decay of the EA order parameter, they suggested that a finite-temperature SG order occurred in  $D = 5$  and 6, but not in  $D \leq 4$ <sup>19</sup>. More recently, the 4D Heisenberg EA model was studied by Coluzzi by equilibrium MC simulation<sup>20</sup>. By examining the behavior of the Binder ratio, she suggested the occurrence of a finite-temperature SG transition in  $D = 4$  in contrast to the suggestion of Ref.<sup>19</sup>. There seems to be no consensus as to the point (i).

The point (ii) above is closely related to the controversy regarding whether the spin-glass and the chiral-glass orders occur simultaneously or separately in 3D. To the authors' knowledge, concerning the chiral-glass order in  $D \geq 4$  dimensions, no calculation has been reported so far. In the present paper, we wish to fill this gap. We study both the spin-glass and the chiral-glass orders of the Heisenberg EA model in both 4D and 5D by means of a large-scale equilibrium MC simulation. In particular, we simulate larger lattices and lower temperatures than those covered in Ref.<sup>20</sup>. For comparison, a simulation is also performed on the mean-field Heisenberg SK model corresponding to  $D = \infty$ .

Our data suggest that, in 5D, the model exhibits a single SG transition at a finite temperature reminiscent to the one of the Heisenberg SK model. The chirality orders simultaneously with the spin, but it behaves as the composite operator of the spin, not as the order parameter. The SG ordered state in 5D accompanies a peculiar type of RSB, most probably a one-step-like RSB, which is different in character from the full RSB realized in the SK model. In 4D, by contrast, the model exhibits a pure chiral-glass transition at a finite temperature, not accompanying the standard SG order. The critical region associated with the chiral-glass transition, however, is very narrow, suggesting that the 4D model lies close to the marginal dimensionality. The chiral-glass ordered state accompanies a one-step-like RSB.

The present paper is organized as follows. In §II, we introduce our model and explain some of the details of the MC calculation. Various physical quantities calculated in our MC simulation are defined in §III. The results of our MC simulation on the 4D, 5D and SK models are presented in §IV. Section V is devoted to summary and discussion.

## II. THE MODEL AND THE METHOD

The model we consider is the isotropic classical Heisenberg model on a 4D or 5D hypercubic lattice, with the nearest-neighbor Gaussian coupling. The Hamiltonian is given by

$$\mathcal{H} = - \sum_{\langle ij \rangle} J_{ij} \vec{S}_i \cdot \vec{S}_j, \quad (1)$$

where  $\vec{S}_i = (S_i^x, S_i^y, S_i^z)$  is a three-component unit vector, and  $\langle ij \rangle$  sum is taken over nearest-neighbor pairs on the lattice. The nearest-neighbor coupling  $J_{ij}$  is assumed to obey the Gaussian distribution with a zero mean and a variance  $J^2$ .

For comparison, we also simulate the corresponding infinite-ranged model, *i.e.*, the Heisenberg SK model corresponding to  $D \rightarrow \infty$ . In the SK model, the Gaussian coupling  $J_{ij}$  works between all possible pairs of total  $N$  spins with a zero mean and a variance  $J^2/N$ .

We perform an equilibrium MC simulation on these models. In 4D, the lattices studied are the hypercubic lattices with  $N = L^4$  sites with  $L = 4, 6, 8$ , and 10, whereas in 5D,  $N = L^5$  with  $L = 3, 4, 5, 6$  and 7. In the case of the SK model,  $N$  is taken to be  $N = 32, 64, 128, 256$  and 512. In all cases, we impose periodic boundary conditions in all  $D$  directions. The sample average is taken over 64-200 independent bond realizations, depending on the system size  $L$  and the lattice dimensionality  $D$ . Error bars of physical quantities are estimated by the sample-to-sample statistical fluctuation over the bond realizations.

In order to facilitate efficient thermalization, we combine the standard heat-bath method with the temperature-exchange technique<sup>21</sup>. Care is taken to be sure that the system is fully equilibrated. Equilibration is checked by the following procedures. First, we monitor the system to travel back and forth many times along the temperature axis during the temperature-exchange process (typically more than 10 times) between the maximum and minimum temperature points. We check at the same time that the relaxation due to the standard heat-bath updating is reasonably fast at the highest temperature, whose relaxation time is of order  $10^2$  Monte Carlo steps per spin (MCS). This guarantees that different parts of the phase space are sampled in each “cycle” of the temperature-exchange run. Second, we check the stability of the results against at least three times longer runs for a subset of samples. Third, we use the method recently developed in Refs.<sup>22,23</sup> for the Gaussian coupling, in which a certain quantity is calculated in two ways, each of which is expected to approach the asymptotic equilibrium value either from above or from below. Further details of our MC simulation are given in Table I.

TABLE I: Detailed conditions of the MC simulation. Here,  $D$  represents the spatial dimensionality,  $N$  the total number of spins,  $N_{\text{samp}}$  the total number of samples,  $N_T$  the total number of temperature points used in the temperature-exchange run,  $T_{\text{max}}/J$  and  $T_{\text{min}}/J$  the maximum and minimum temperatures in the temperature-exchange run.

$D$	$N$	$N_{\text{samp}}$	$N_T$	$T_{\text{max}}/J$	$T_{\text{min}}/J$
4	$4^4$	140	20	1.0	0.16
	$6^4$	100	34	0.65	0.21
	$8^4$	80	50	0.58	0.21
	$10^4$	80	50	0.48	0.256
5	$3^5$	120	24	1.2	0.24
	$4^5$	100	36	1.0	0.3
	$5^5$	96	46	0.8	0.31
	$6^5$	96	56	0.75	0.40
	$7^5$	64	50	0.75	0.537
$\infty(\text{SK})$	32	200	30	0.5	0.1
	64	200	30	0.5	0.1
	128	200	30	0.5	0.1
	256	100	34	0.5	0.1
	512	100	34	0.5	0.1

### III. PHYSICAL QUANTITIES

In this section, we define various physical quantities calculated in our simulation below.

#### A. Spin-related quantities

By considering two independent systems (“replicas”) described by the same Hamiltonian (1), one can define an overlap variable. The overlap of the Heisenberg spin is defined as a *tensor* variable  $q_{\mu\nu}$  between the  $\mu$  and  $\nu$  components ( $\mu, \nu=x, y, z$ ) of the Heisenberg spin,

$$q_{\mu\nu} = \frac{1}{N} \sum_{i=1}^N S_{i\mu}^{(1)} S_{i\nu}^{(2)} \quad , \quad (\mu, \nu = x, y, z) \quad , \quad (2)$$

where  $\vec{S}_i^{(1)}$  and  $\vec{S}_i^{(2)}$  are the  $i$ -th Heisenberg spins of the replicas 1 and 2, respectively. In our simulation, we prepare the two replicas 1 and 2 by running two independent sequences of systems in parallel with different spin initial conditions and different sequences of random numbers. In terms of these tensor overlaps, the SG order parameter is defined by

$$q_s^{(2)} = [\langle q_s^2 \rangle] \quad , \quad q_s^2 = \sum_{\mu, \nu=x, y, z} q_{\mu\nu}^2 \quad , \quad (3)$$

while the associated spin Binder ratio is defined by

$$g_s = \frac{1}{2} \left( 11 - 9 \frac{[\langle q_s^4 \rangle]}{[\langle q_s^2 \rangle]^2} \right) \quad , \quad (4)$$

where  $\langle \dots \rangle$  represents the thermal average and  $[\dots]$  the average over the bond disorder. Note that  $g_s$  is normalized here so that, in the thermodynamic limit, they vanish in the high-temperature phase and gives unity in the nondegenerate ordered state.

The spin-overlap distribution function is originally defined in the tensor space, since the relevant spin-overlap has  $3 \times 3 = 9$  independent components. For the convenience of illustration, we introduce here the diagonal spin-overlap distribution function,

$$P_s(q'_{\text{diag}}) = [\langle \delta(q'_{\text{diag}} - q_{\text{diag}}) \rangle] \quad , \quad (5)$$

defined in terms of the diagonal overlap  $q_{\text{diag}}$  which is the trace of the tensor overlap  $q_{\mu\nu}$ 's,

$$q_{\text{diag}} = \sum_{\mu=x,y,z} q_{\mu\mu} = \frac{1}{N} \sum_{i=1}^N \vec{S}_i^{(1)} \cdot \vec{S}_i^{(2)} . \quad (6)$$

Note that the spin Binder ratio Eq.(4) is defined from the full tensor overlap distribution function, but cannot be derived solely from the diagonal overlap distribution function Eq.(6).

In zero field, the distribution function  $P_s(q_{\text{diag}})$  is symmetric with respect to  $q_{\text{diag}} = 0$ . In the high-temperature phase, each  $q_{\mu\nu}$  ( $\mu, \nu = x, y, z$ ) is expected to be Gaussian-distributed around  $q_{\mu\nu} = 0$  in the  $L \rightarrow \infty$  limit, and so is  $q_{\text{diag}}$ . In the hypothetical SG ordered state, reflecting the fact that  $q_{\text{diag}}$  transforms nontrivially under the independent global  $O(3)$  spin rotations on the two replicas, even a self-overlap part of  $P_s(q_{\text{diag}})$  develops a nontrivial shape, *i.e.*, it is not a simple delta-function located at the EA SG order parameter  $\pm q_s^{\text{EA}}$ . Hence, we need to clarify first how the function  $P_s(q_{\text{diag}})$  looks like in the possible SG ordered state with a nonzero  $\pm q_s^{\text{EA}}$ .

Let us hypothesize here that there exists a *spin*-glass ordered state characterized by a nonzero EA SG order parameter  $q_s^{\text{EA}} > 0$ . One can show in the  $L \rightarrow \infty$  limit that the self-overlap part of  $P_s(q_{\text{diag}})$  is given by

$$P_s(q_{\text{diag}}) = \frac{3\sqrt{3}}{4\pi q_s^{\text{EA}}} \left( \sqrt{\frac{q_s^{\text{EA}} - q_{\text{diag}}}{3q_{\text{diag}} + q_s^{\text{EA}}}} + \sqrt{\frac{q_s^{\text{EA}} + q_{\text{diag}}}{-3q_{\text{diag}} + q_s^{\text{EA}}}} \right) , \quad (7)$$

which is illustrated in Fig.1. The derivation of Eq.(7) is given in the Appendix. Note that diverging  $\delta$ -function peaks appear at  $q_{\text{diag}} = \pm \frac{1}{3}q_s^{\text{EA}}$ , not at  $q_{\text{diag}} = \pm q_s^{\text{EA}}$ . If the SG ordered state accompanies RSB, the associated nontrivial contribution would be added to the one given by Eq.(7). In any case, an important observation here is that, as long as the ordered state possesses a finite SG long-range order (LRO), the diverging peak should arise in  $P_s(q_{\text{diag}})$  at  $q_{\text{diag}} = \pm \frac{1}{3}q_s^{\text{EA}}$ .

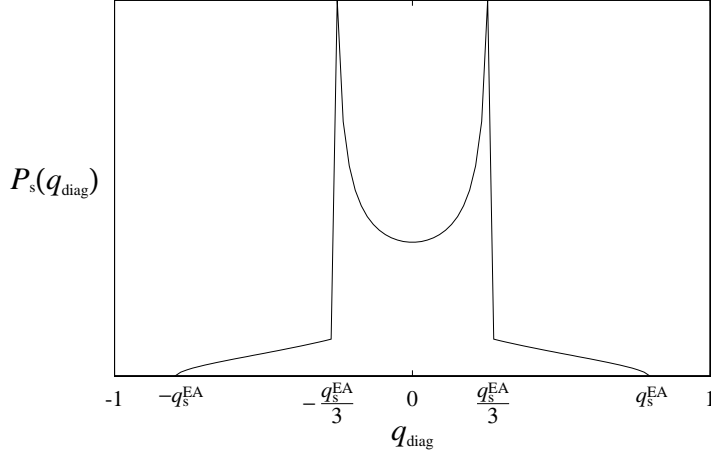


FIG. 1: Sketch of the self-overlap part of the diagonal spin-overlap distribution function  $P_s(q_{\text{diag}})$  in the thermodynamic limit, expected when there exists a finite SG long-range order with a nonzero  $q_s^{\text{EA}} > 0$ .

## B. Chirality-related quantities

We define the local chirality at the  $i$ -th site and in the  $\mu$ -th direction,  $\chi_{i\mu}$ , for three neighboring Heisenberg spins by the scalar

$$\chi_{i\mu} = \vec{S}_{i+\hat{e}_\mu} \cdot (\vec{S}_i \times \vec{S}_{i-\hat{e}_\mu}) , \quad (8)$$

where  $\hat{e}_\mu$  ( $\mu = x_1, x_2, \dots, x_D$ ) denotes a unit vector along the  $\mu$ -th axis. By this definition, there are in total  $DN$  local chiral variables.

In the case of the SK model, since there is no “neighbors” in the model, the definition of the local chirality accompanies some difficulties. Here, just for convenience, we number the  $N$  spins arbitrarily, and define the local chirality by

$$\chi_i = \vec{S}_{i+1} \cdot (\vec{S}_i \times \vec{S}_{i-1}) . \quad (9)$$

Then, there are in total  $N$  chiral variables.

The mean local amplitude of the chirality,  $\bar{\chi}$ , may be defined by

$$\bar{\chi} = \sqrt{\frac{1}{DN} \sum_{i=1}^N \sum_{\mu=x_1, x_2, \dots, x_D} [\langle \chi_{i\mu}^2 \rangle]} , \quad (10)$$

for  $D = 4$  and  $5$ , and by

$$\bar{\chi} = \sqrt{\frac{1}{N} \sum_{i=1}^N [\langle \chi_i^2 \rangle]} , \quad (11)$$

for the SK model. Note that the magnitude of  $\bar{\chi}$  tells us the extent of the noncoplanarity of the local spin structures. In particular, this quantity vanishes for any coplanar spin configuration.

As in the case of the Heisenberg spin, one can define an overlap of the chiral variable by considering the two replicas. In the cases of  $D = 4$  and  $5$ , it is defined by

$$q_\chi = \frac{1}{DN} \sum_{i=1}^N \sum_{\mu=x_1, x_2, \dots, x_D} \chi_{i\mu}^{(1)} \chi_{i\mu}^{(2)} , \quad (12)$$

where  $\chi_{i\mu}^{(1)}$  and  $\chi_{i\mu}^{(2)}$  represent the chiral variables of the replicas 1 and 2, respectively. In the case of the SK model, it is defined by

$$q_\chi = \frac{1}{N} \sum_{i=1}^N \chi_i^{(1)} \chi_i^{(2)} . \quad (13)$$

In terms of this chiral overlap  $q_\chi$ , the chiral-glass order parameter is defined by

$$q_\chi^{(2)} = [\langle q_\chi^2 \rangle] . \quad (14)$$

The associated chiral-glass susceptibility may be defined by

$$\chi_\chi = DN [\langle q_\chi^2 \rangle] , \quad (15)$$

in the cases of  $D = 4$  and  $5$ , while in the case of the SK model, it is defined by

$$\chi_\chi = N [\langle q_\chi^2 \rangle] . \quad (16)$$

Unlike the spin variable, the local magnitude of the chirality is somewhat temperature dependent. In order to take account of this effect, we also consider the reduced chiral-glass susceptibility  $\tilde{\chi}_\chi$  by dividing  $\chi_\chi$  by the appropriate powers of  $\bar{\chi}$ ,

$$\tilde{\chi}_\chi = \frac{\chi_\chi}{\bar{\chi}^4} . \quad (17)$$

The Binder ratio of the chirality is defined by

$$g_\chi = \frac{1}{2} \left( 3 - \frac{[\langle q_\chi^4 \rangle]}{[\langle q_\chi^2 \rangle]^2} \right) . \quad (18)$$

The distribution function of the chiral overlap  $q_\chi$  is defined by

$$P_\chi(q'_\chi) = [\langle \delta(q'_\chi - q_\chi) \rangle] . \quad (19)$$

## IV. MONTE CARLO RESULTS

In this section, we present our MC results on the Heisenberg EA models in 4D, 5D, and in the SK limit (corresponding to  $D = \infty$ ).

### A. Chiral Binder ratio

In Fig.2, we show the Binder ratio of the chirality in the cases of (a) 4D, (b) 5D and (c) the SK model, respectively. In all these cases,  $g_\chi$  exhibits a negative dip, while its temperature and size dependence is somewhat different from each other.

In 4D, with increasing the lattice size  $L$ , the negative dip tends to deepen while the dip temperature  $T_{\text{dip}}$  is almost kept constant at around  $T/J = 0.38$ : See the inset of Fig.2. One can also see from Fig.2 that  $g_\chi$  for various  $L$  cross in the negative region of  $g_\chi$  at temperatures slightly above  $T_{\text{dip}}$ . The occurrence of a negative dip deepening with  $L$ , accompanied by a crossing on the negative side of  $g_\chi$ , is similar to the one previously observed in the corresponding 3D model<sup>10,11,12</sup>, although, in 3D,  $T_{\text{dip}}$  tends to shift toward lower temperature with increasing  $L$ . As argued in Ref.<sup>10,11,12</sup>, the occurrence of a negative dip deepening with  $L$  is a signature of the occurrence of a phase transition in the chiral sector. By making a linear extrapolation of  $T_{\text{dip}}(L)$  with respect to  $L^{-1}$ , as shown in the inset of Fig.2 (a), we estimate the bulk chiral-glass transition temperature as  $T_{\text{CG}}/J = 0.38(2)$ . Below  $T_{\text{CG}}$ , the curves for  $L \geq 6$  almost merge into a curve exhibiting the nontrivial temperature dependence. Such a behavior suggests that the chiral ordered state accompanies a nontrivial phase-space structure, *i.e.*, RSB.

In 5D, although the negative dip tends to deepen up to the size  $L = 5$ , it tends to become shallower for  $L \geq 6$ . In contrast to the 3D and 4D cases, the dip temperature  $T_{\text{dip}}$  tends to shift toward higher temperature with increasing  $L$ . The observed temperature and size dependence of  $g_\chi$  strongly suggests again that the limit  $T_{\text{dip}}(L \rightarrow \infty)$  corresponds to a transition temperature in the chiral sector. The  $1/L$ -extrapolation of  $T_{\text{dip}}(L)$  to  $L \rightarrow \infty$ , shown in the inset of Fig.2 (b), yields the estimate  $T_{\text{CG}}/J = 0.62(2)$ .

In the SK case, the negative dip of  $g_\chi$  becomes shallower with increasing  $L$ , and  $T_{\text{dip}}$  shifts toward higher temperature. In the inset,  $T_{\text{dip}}(N)$  is plotted as a function of  $N^{-1/325,26}$ , which yields  $T_{\text{CG}}/J = 0.31(2)$ . The estimated chiral-glass ordering temperature agrees within errors with the exactly-known SG transition temperature of the Heisenberg SK model,  $T_{\text{SG}}/J = 1/3$ . This coincidence simply confirms the fact that, at the SG transition of the Heisenberg SK model, Heisenberg spins order in a noncoplanar manner, which necessarily accompanies the onset of a nonzero chiral-glass LRO. As is evident, in the SK case, the order parameter of the transition is not the chirality, but the Heisenberg spin itself.

### B. Chiral autocorrelation function

More direct measure of the chiral-glass transition may be obtained from the equilibrium dynamics of the model. We compute the autocorrelation function of the chirality defined by

$$C_\chi(t) = \frac{1}{DN} \sum_{i=1}^N \sum_{\mu=x_1, x_2, \dots, x_D} [\langle \chi_{i\mu}(t_0) \chi_{i\mu}(t + t_0) \rangle] \quad , \quad (20)$$

where the “time”  $t$  is measured here in units of MCS. In computing (20), the simulation is performed according to the standard heat-bath updating without the temperature-exchange procedure, while the starting spin configuration at  $t = t_0$  is taken from the equilibrium spin configurations generated in our temperature-exchange MC runs.

We show in Fig.3 the time dependence of  $C_\chi(t)$  on a log-log plot for the cases of (a) 4D, and (b) 5D. To check the possible size dependence, the data for the two largest lattice sizes are given together, one denoted by symbols and the other by thin lines. In the chiral-glass ordered state with a nonzero  $q_\chi^{\text{EA}}$ ,  $C_\chi(t)$  in the  $L \rightarrow \infty$  limit should exhibit an upward curvature, tending to  $q_\chi^{\text{EA}} > 0$ . In the disordered phase,  $C_\chi(t)$  should exhibit a downward curvature. Just at  $T = T_{\text{CG}}$ , the linear behavior corresponding to the power-law decay is expected. As shown in the figures, in the time region where the finite-size effect is negligible,  $C_\chi(t)$  shows either a downward curvature characteristic of the disordered phase, or an upward curvature characteristic of the ordered phase, depending on whether the temperature is higher or lower than a critical value. In 4D, the chiral-glass transition temperature estimated in this way is  $T_{\text{CG}}/J = 0.38(2)$ , while in 5D it is  $T_{\text{CG}}/J = 0.60(2)$ . Both are close to our estimate above based on the chiral Binder ratio. Our observation that  $C_\chi(t)$  exhibits an upward curvature below  $T_{\text{CG}}$  indicates that the chiral-glass ordered state is “rigid” with a nonzero long-range order parameter.

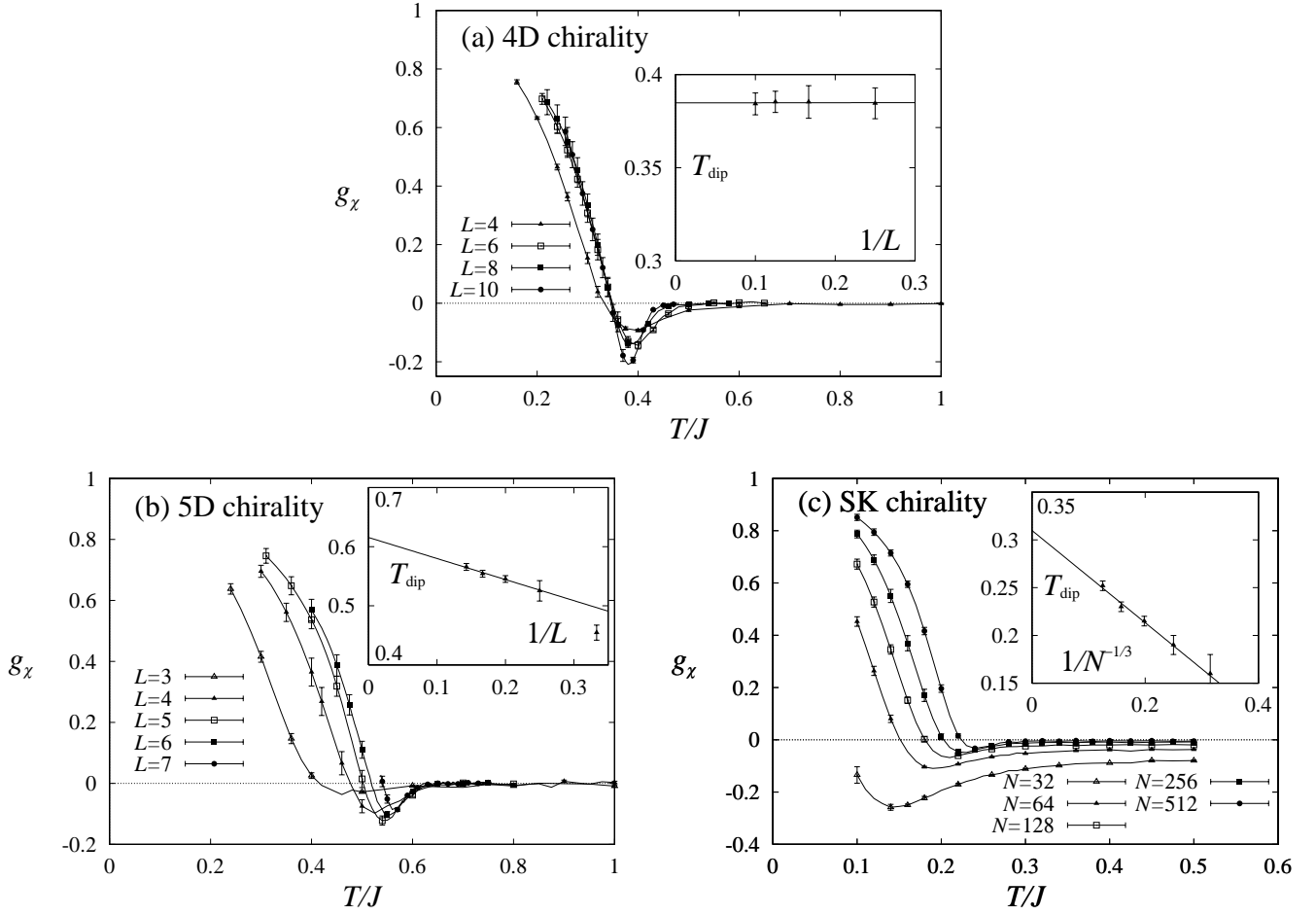


FIG. 2: Temperature and size dependence of the chiral Binder ratio  $g_\chi$  in 4D (a), in 5D (b), and in the SK model (c). In the insets,  $T_{\text{dip}}$  is plotted versus  $1/L$  (or versus  $1/N^{-1/3}$  in the case of the SK model).

From the above analysis, the occurrence of the chiral-glass LRO in 4D and 5D seems now well established. The next question is whether the chiral-glass order accompanies the standard SG order. If the SG order occurs at the same temperature as the chiral-glass order, the transition is likely to be of the standard type, at least in the sense that the order parameter of the transition is the spin, not the chirality. (Here, recall that the SG ordered state in the Heisenberg SG inevitably accompanies the chiral-glass order as long as the spin is frozen in a noncoplanar manner.) By contrast, if the SG order occurs at a temperature below the ordering temperature of the chirality, it means the unusual situation, *i.e.*, the occurrence of the spin-chirality decoupling, the pure chiral-glass transition and the pure chiral-glass ordered state. To clarify this issue, we examine the spin Binder ratio in the next subsection.

### C. Spin Binder ratio

In Fig.4, we show the temperature and size dependence of the Binder ratio of the spin in the cases of (a) 4D, (b) 5D and (c) the SK model. In each figure, magnified figure is embedded to show the detailed behavior of  $g_s$  in the region of interest. The arrow in each figure indicates the location of the transition point of the chirality determined above. In 4D, as can be seen from Fig.4 (a),  $g_s$  for the range of sizes  $4 \leq L \leq 8$  appears to almost merge at a temperature  $T/J \simeq 0.4$  close to the chiral-glass transition temperature determined above. This seems to suggest that the spin sector also becomes critical at  $T \simeq T_{\text{CG}}$ , which may indicate the simultaneous spin-glass and chiral-glass transition at  $T/J \simeq 0.4$ . Quite remarkably, however, the spin Binder ratio  $g_s$  for our largest size  $L = 10$  comes definitely below the curves for  $L \leq 8$ . In fact, the  $L = 10$  curve lies below the  $L \leq 8$  curves more than four sigmas, and the observed

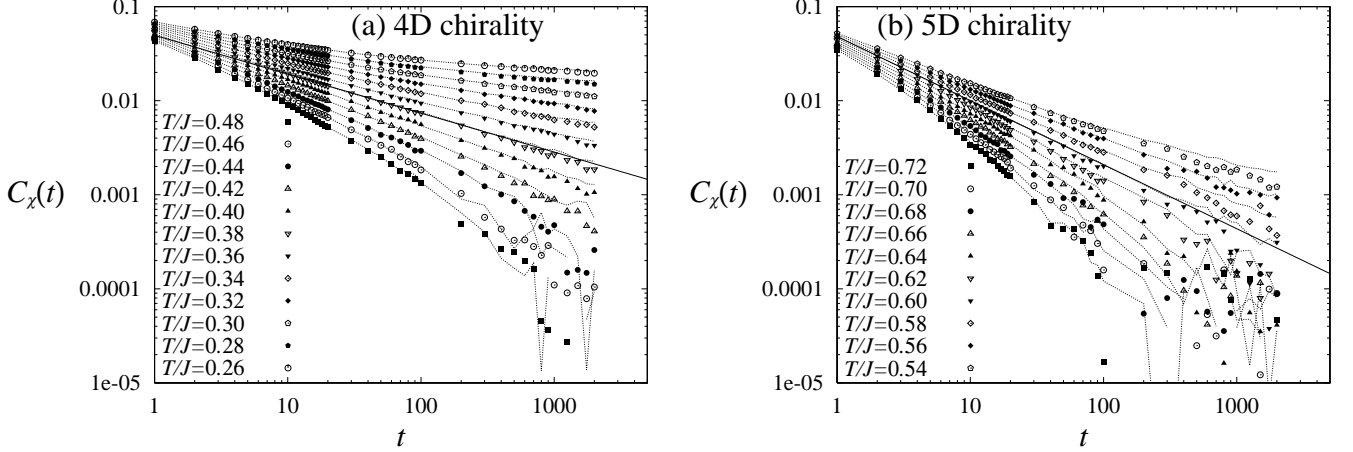


FIG. 3: Temporal decay of the equilibrium chiral autocorrelation function at various temperatures in 4D (a), and in 5D (b). In (a), symbols represent the data of  $L = 8$  and thin lines those of  $L = 10$ . In (b), symbols represent the data of  $L = 6$  and thin lines those of  $L = 7$ . Solid straight lines represent the power-law fits of the data at  $T/J = 0.38$  (a), and at  $T/J = 0.60$  (b).

departure is statistically well significant. From this observation, we conclude that, although the spin sector once becomes near-critical at the chiral-glass transition  $T = T_{CG}$  on short length scales, it eventually remains off-critical (paramagnetic) at  $T = T_{CG}$  on longer length scales. Namely, the spin-chirality decoupling previously observed in 3D in Ref.<sup>10</sup> seems to come into play in 4D as well, which keeps the spin sector being paramagnetic even below  $T = T_{CG}$ . If this is the case, the transition in 4D is a pure chiral-glass transition and the ordered state is a pure chiral-glass state not accompanying the standard SG order. Even in certain temperature range below  $T_{CG}$ ,  $g_s$  is expected to approach zero in the  $L \rightarrow \infty$  limit, which seems consistent with the present data. We interpret the strange structure observed in  $g_s$  near  $T = T_{CG}$  for larger  $L$  as a remanence of the near-critical behavior of the spin at the chiral-glass transition. Meanwhile, due to the lack of our data in the lower temperature region  $T/J \lesssim 0.2$ , it is difficult to determine from the present data whether the SG transition occurs either only at zero temperature,  $T_{SG} = 0$ , or at a finite temperature below the chiral-glass transition temperature,  $0 < T_{SG} < T_{CG}$ . Nevertheless, Fig.4(a) strongly suggests that  $T_{SG}$ , if it is nonzero, is less than  $0.2J$ .

We note in passing that the spin Binder ratio  $g_s$  of the same 4D model was calculated by Coluzzi for smaller sizes  $L = 3, 4$  and  $5$  and at higher temperatures  $T/J \geq 0.5$ <sup>20</sup>. She observed that  $g_s$  for  $L = 3, 4$  and  $5$  appeared to merge around  $T/J \simeq 0.5$ , and suggested that there occurred a standard SG transition at  $T/J \simeq 0.5$ . In the present calculation made for larger lattice sizes and for lower temperatures, although we indeed observed a near-merging behavior of  $g_s$ , it occurred at a temperature  $T/J \simeq 0.4$  near  $T_{CG}$ , somewhat lower than the estimate of Ref.<sup>20</sup>, and most importantly,  $g_s$  for larger lattices show clear deviation from the merging behavior, suggesting that the Heisenberg spin remains paramagnetic even below the chiral-glass transition point.

Now, we turn to the spin Binder ratio in 5D. As shown in Fig.4 (b),  $g_s$  for  $3 \leq L \leq 7$  show a crossing at a temperature around  $T/J \simeq 0.60$ , strongly suggesting that the SG order occurs at  $T_{SG}/J = 0.60(2)$ . At lower temperatures,  $g_s$  for larger  $L$  tends to come down again, exhibiting a behavior reminiscent to the one observed in 4D. In particular, at low enough temperatures,  $g_s$  decreases with  $L$ . The observed non-monotonic temperature dependence and the peculiar size dependence of  $g_s$  below  $T_{SG}$  suggests that the SG state below  $T_{SG}$  might be a nontrivial one accompanied by a peculiar RSB, possibly the one-step-like one as observed in the chirality sector.

In the SK case, the calculated  $g_s$  exhibits a clear crossing behavior at around  $T/J = 1/3$ , an exactly known SG transition temperature of the model. At lower temperatures,  $g_s$  monotonically increases with  $N$  in contrast to the 4D and 5D cases, and eventually appear to converge to the temperature-dependent values less than unity. The observation that the asymptotic  $g_s(L \rightarrow \infty)$  in the region  $0 < T < \frac{1}{3}J = T_{SG}$  differs from unity reflects the fact that the SG ordered state of the SK model accompanies a full (or hierarchical) RSB.



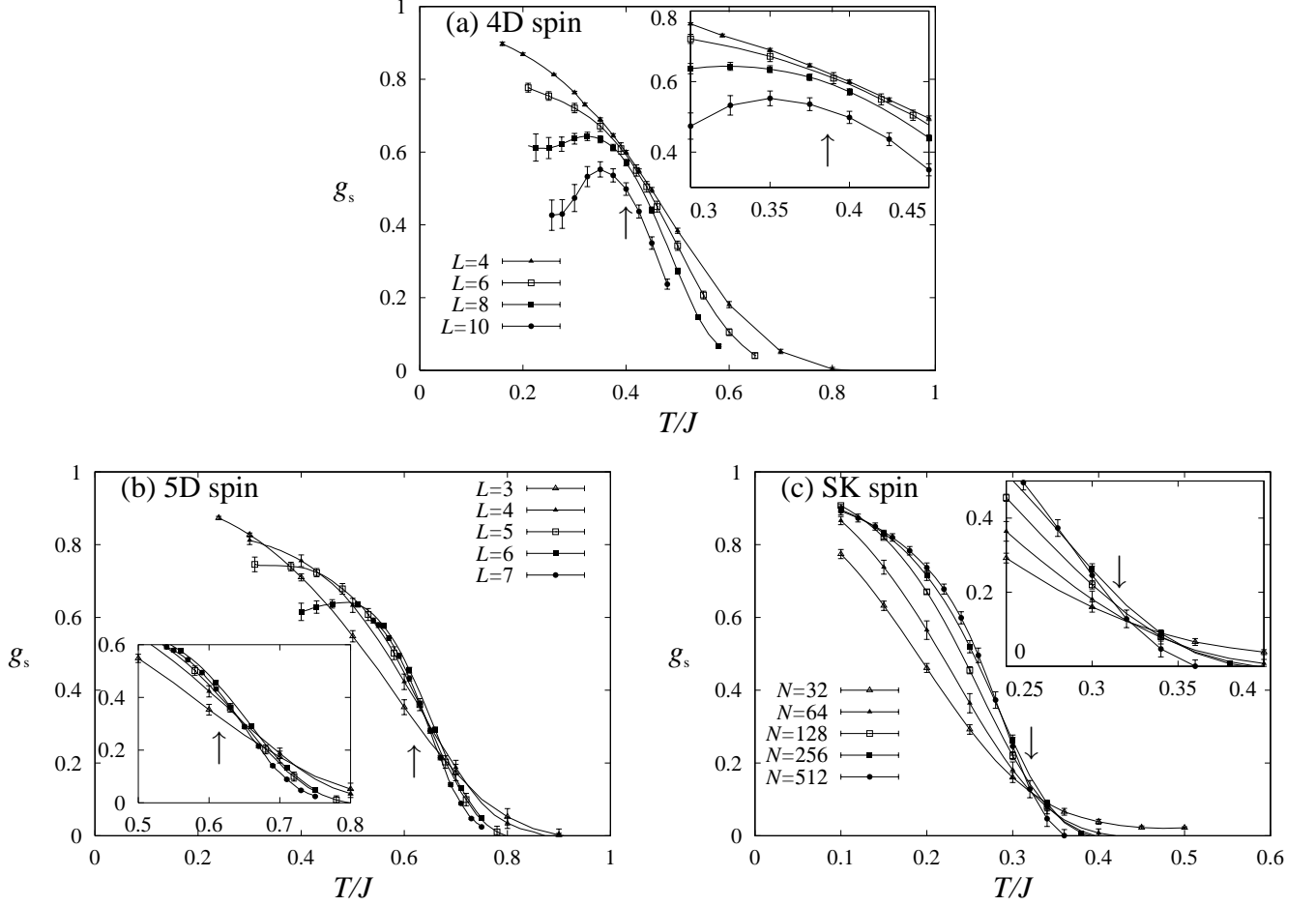


FIG. 4: Temperature and size dependence of the spin Binder ratio  $g_s$  in 4D (a), in 5D (b), and in the SK model (c). Magnified figures are given as insets. The arrow in each figure represents the location of the chiral-glass transition point.

#### D. Chiral overlap distribution function

In Fig.5, we show the overlap distribution function of the chirality,  $P_\chi(q_\chi)$ , well below  $T_{CG}$ , at around  $T \simeq \frac{2}{3}T_{CG}$ . In 4D, in addition to the "side peaks" corresponding to  $q_\chi = \pm q_\chi^{EA}$  which grow and sharpen with increasing  $L$ , a "central peak" appears at  $q_\chi = 0$  for  $L \geq 6$ , which also sharpens and gets higher with increasing  $L$ . These features were reminiscent to the ones observed in 3D, which was interpreted as a signature of the one-step-like RSB in the chiral-glass ordered state<sup>10,11,12</sup>. Our present data suggest that the chiral-glass state in 4D also accompanies the one-step-like RSB as in the 3D case. This is fully consistent with the observed behavior of the chiral Binder ratio.

A central peak in  $P_\chi(q_\chi)$  is also observed in 5D in the largest lattice size  $L = 6$ . This suggests the occurrence of the one-step-like RSB also in 5D.

In the SK case, the calculated  $P_\chi(q_\chi)$  exhibits the side peaks at  $q_\chi = \pm q_\chi^{EA}$  only, without a central peak at  $q_\chi = 0$  for any size studied. Instead, the value of  $P_\chi(0)$  gradually decreases with increasing  $N$ , where  $1/N$ -extrapolation of  $P_\chi(0)$  to  $N \rightarrow \infty$  gives a nonzero value,  $P_\chi(q_\chi = 0, N = \infty) \simeq 6.0 \times 10^{-4}$ . Thus, in the SK case, the chirality exhibits the standard full RSB, in apparent contrast to the 4D and 5D cases.

#### E. Spin overlap distribution function

In Fig.6, we show the diagonal spin-overlap distribution function,  $P_s(q_{diag})$ , for the cases of (a) 4D, (b) 5D and (c) the SK model. The temperatures are taken to be the same as those for the chiral overlap distribution shown in Fig.6,

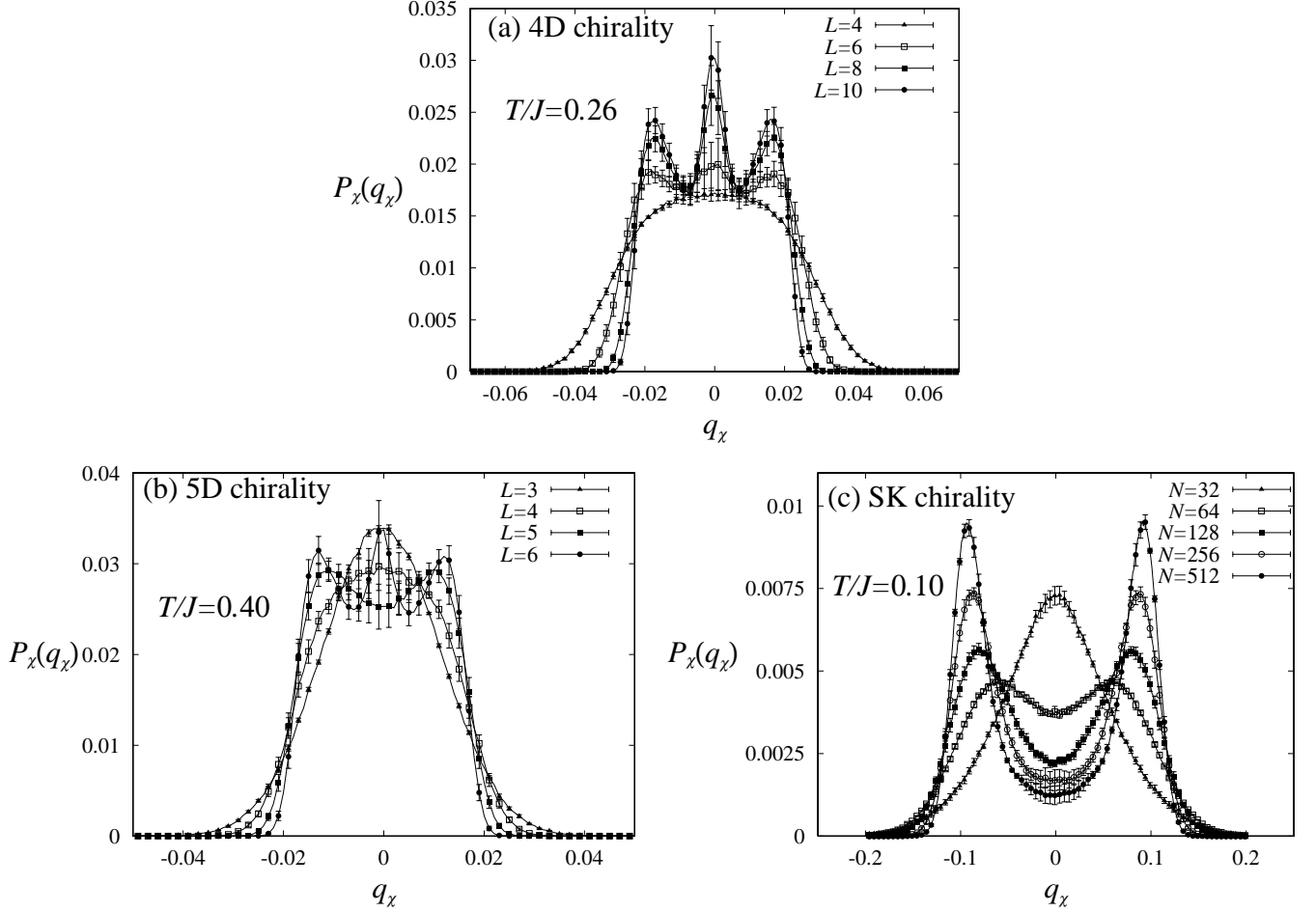


FIG. 5: Overlap distribution function of the chirality, in 4D at  $T/J = 0.26$  (a), in 5D at  $T/J = 0.40$  (b), and in the SK model at  $T/J = 0.10$  (c).

*i.e.*, about  $\frac{2}{3}T_{CG}$ .

In the SK case shown in Fig.6(c), the shape of  $P_s(q_{\text{diag}})$  is similar to the one of Fig.1, with symmetric diverging peaks observed at  $q_{\text{diag}} \simeq \pm 0.2$ . These peaks are then identified with the ones expected at  $\pm \frac{1}{3}q_s^{\text{EA}}$  when there is a finite SG LRO. This observation is fully consistent with the fact that the standard SG LRO with a nonzero  $q_s^{\text{EA}}$  is realized in the ordered state of the SK model. In 5D, the growing symmetric peaks also appear at  $q_{\text{diag}} \simeq \pm 0.18$  for  $L \geq 5$ , suggesting that the SG LRO characterized by a nonzero  $q_s^{\text{EA}}$  is realized.

In 4D, by contrast, no peaks corresponding to  $\pm \frac{1}{3}q_s^{\text{EA}}$  are observed, at least within the range of sizes we simulate. Instead,  $P_s(q_{\text{diag}})$  exhibits a marginal behavior, staying nearly flat with a plateau-like structure at  $|q_{\text{diag}}| \lesssim 0.2$  for  $L \geq 6$ . With increasing  $L$ , this plateau gradually gets higher but no side peaks show up. Since the normalization condition of  $P_s(q_{\text{diag}})$  inhibits the plateau of finite width getting higher indefinitely, one plausible asymptotic behavior of  $P_s(q_{\text{diag}})$  might be that it eventually converges in the  $L \rightarrow \infty$  limit to the Gaussian distribution around  $q_{\text{diag}} = 0$ . In that sense, the observed behavior is consistent with the spin disorder at this temperature. However, solely from the present data, we cannot completely rule out the possibility that the  $\pm q_s^{\text{EA}}/3$  peaks characteristic of the SG LRO eventually show up for still larger  $L$ . Anyway, in the range of sizes studied  $L \leq 10$ , we have observed no sign of such side peaks, in contrast to the 5D case where the side peaks appear already for  $L = 5$ . Another possibility may be that the 4D model exhibits a finite-temperature SG transition but the SG state is a critical phase with a vanishing SG order parameter  $q_s^{\text{EA}} = 0$ , as expected for the system at its LCD. However, as argued below, such a LCD behavior is not supported from our data of the critical properties.

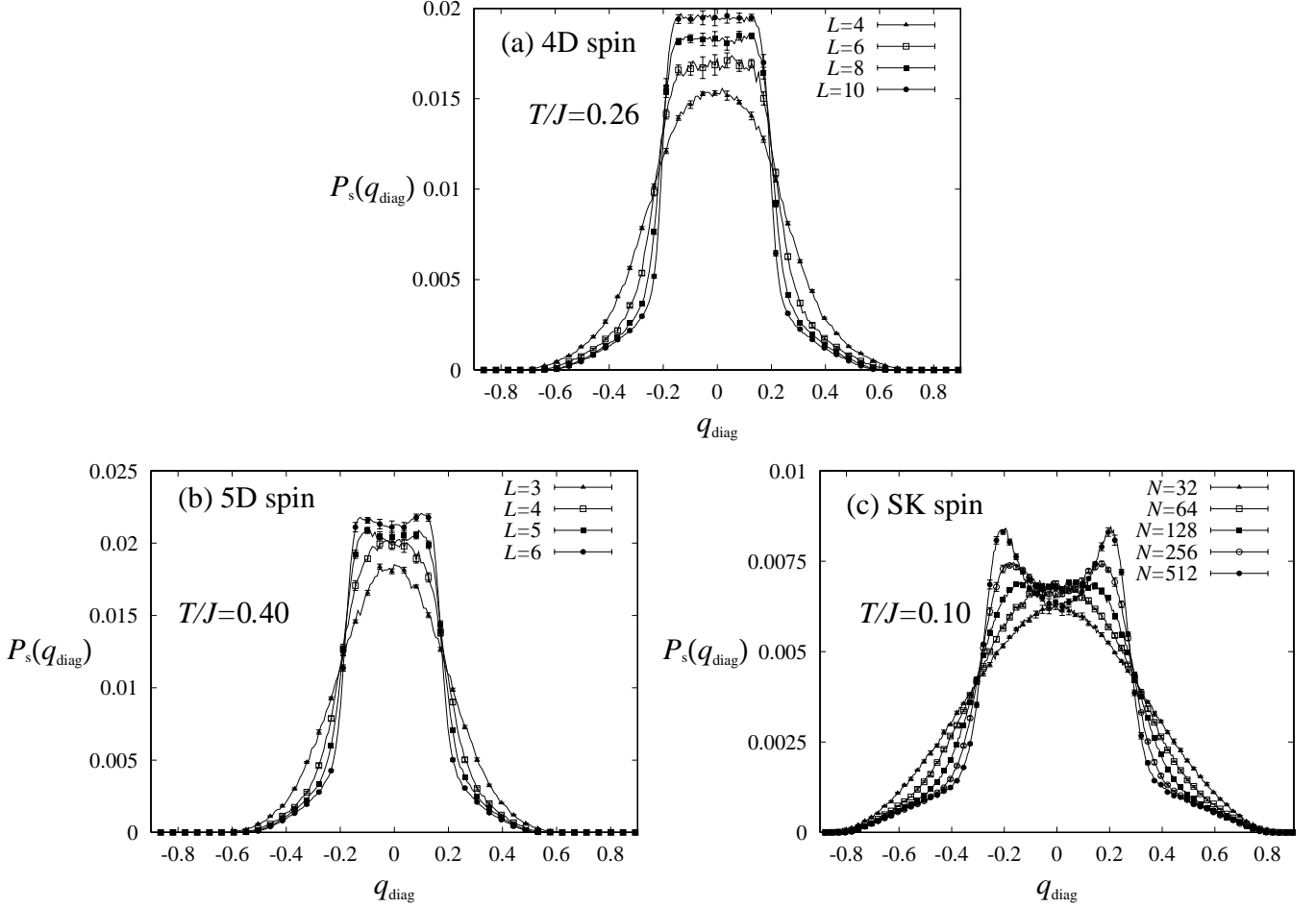


FIG. 6: Overlap distribution function of the diagonal part of the spin, in 4D at  $T/J = 0.26$  (a), in 5D at  $T/J = 0.40$  (b), and in the SK model at  $T/J = 0.10$  (c).

### F. Chiral-glass susceptibility

From the data presented above, we have concluded that in 4D the chirality is an order parameter of the transition, but not so in 5D and in the SK model: In the latter cases, the order parameter of the transition is the spin, while the chirality order is parasitic to the spin order. In order to examine further the validity of such a picture, we show in Figs.7 the temperature and size dependence of the reduced chiral-glass susceptibility, where  $\tilde{\chi}_\chi$  is plotted as a function of the reduced temperature  $(T - T_{\text{CG}})/T_{\text{CG}}$  on a log-log scale. As determined above,  $T_{\text{CG}}$  is taken to be  $T_{\text{CG}}/J = 0.38$  in 4D and  $T_{\text{CG}}/J = 0.60$  in 5D. In the SK case, we put  $T_{\text{CG}}/J = \frac{1}{3}$  which is exact.

As can be seen from Figs.7 (b) and (c), the reduced chiral-glass susceptibilities of the 5D and the SK models do not exhibit any sign of divergence: They stay small at any temperature  $T > T_{\text{CG}}$ , and most notably,  $\tilde{\chi}_\chi$  gets smaller with increasing the system size  $L$ . Such a size dependence is completely opposite to the one expected for a diverging quantity in the critical region. We note that even at temperatures close to the transition temperature, no sign of the reversal of the size dependence is discernible. In fact, in the SK case, such a non-diverging behavior of  $\tilde{\chi}_\chi$  is just as expected. In the SK model, the standard SG exponents are known to be  $\alpha = -1$ ,  $\beta_{\text{SG}} = 1$  and  $\gamma_{\text{SG}} = 1$ . Then the chiral-glass exponent  $\beta_{\text{CG}}$  is expected to be  $\beta_{\text{CG}} = 3$ , because the chirality is cubic in the spin variables. Then, the chiral-glass susceptibility exponent is obtained as  $\gamma_{\text{CG}} = -3$  from the scaling relation  $\alpha + 2\beta_{\text{CG}} + \gamma_{\text{CG}} = 2$ . Negative  $\gamma_{\text{CG}}$  means that the chiral-glass susceptibility of the SK model does not diverge at the SG transition. Very much similar behavior observed in 5D suggests that the the chiral-glass susceptibility of the 5D model does not diverge at the transition, either. Hence, our observations for  $\tilde{\chi}_\chi$  are fully consistent with our previous finding that the order parameter of the transition in 5D and in the SK model is the spin, not the chirality.

By contrast, in 4D,  $\tilde{\chi}_\chi$  exhibits a different behavior. Although in the investigated temperature regime  $\tilde{\chi}_\chi$  stays rather small and tends to decrease with increasing  $L$ , similarly to the behavior observed in 5D and in the SK limit, its size dependence is about to change in a close vicinity of  $T_{CG}$ . More specifically, the  $L = 10$  data catch up the  $L = 8$  data at  $t \simeq 0.04$ , and at temperatures further close to  $T_{CG}$ , exceeds the  $L = 8$  data, where the data show significant finite-size rounding preventing the observation of the asymptotic critical behavior. This suggests that the critical region of the chiral-glass transition might be very narrow in 4D, limited to the regime  $t \lesssim 10^{-2}$ . In the temperature range outside this, the chirality exhibits a mean-field-like non-diverging behavior similar to the one of the SK model. Although we cannot directly get into this narrow critical region in our present simulation due to the computational limitation, the observed behavior of  $\tilde{\chi}_\chi$  of the 4D model indeed suggests that such a crossover from the mean-field-like behavior at  $t \gtrsim 10^{-2}$  to the diverging critical behavior at  $t \lesssim 10^{-2}$  does occur. Unfortunately, inaccessibility to the asymptotic critical region prevents us from estimating the chirality exponents. In order to estimate the asymptotic chiral critical exponents, one needs to approach the temperature regime  $t \lesssim 10^{-2}$  with larger lattices  $L \geq 10$ , which is not feasible with the computational capability presently available to us.

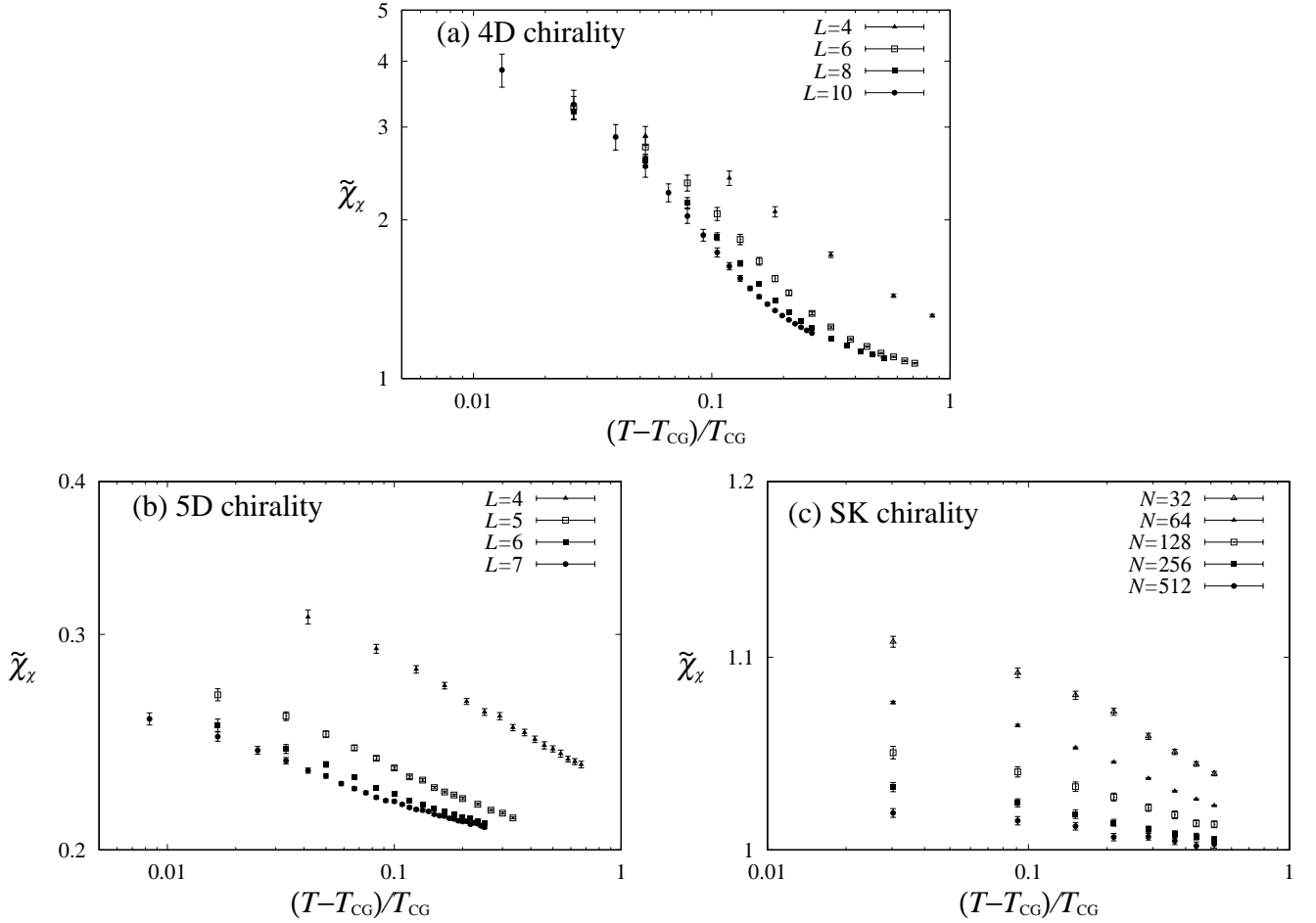


FIG. 7: Temperature and size dependence of the reduced chiral-glass susceptibility in 4D (a), in 5D (b), and in the SK model (c).

### G. Critical Exponents

In this subsection, we analyze the critical properties of the SG transition in each case of 5D and of the SK model. In the case of 4D, our analysis has suggested that the transition is a pure chiral-glass transition, the associated chiral critical regime being narrow,  $t \lesssim 10^{-2}$ , which prevents us from estimating the chiral critical exponents.

In 5D, we have concluded that the transition is the standard SG transition, *i.e.*, the order parameter is the spin, not the chirality, although the chirality also takes a nonzero value in the SG ordered state reflecting the noncoplanar character of the spin order. We estimate the associated SG exponents via the standard finite-size-scaling analysis of  $q_s^{(2)}$ , based on the relation,

$$q_s^{(2)} \approx L^{-(d-2+\eta_{\text{SG}})} f(L^{1/\nu_{\text{SG}}} |T - T_{\text{SG}}|) \quad , \quad (21)$$

where the  $T_{\text{SG}}$  value is set to the best value determined above,  $T_{\text{SG}}/J = 0.60$ . The best estimates of the SG exponents are  $\nu_{\text{SG}} = 0.6(2)$  and  $\eta_{\text{SG}} = -0.8(2)$ : See Fig.8. From the standard scaling relation, we get other exponents as  $\alpha = -1.0(5)$ ,  $\beta_{\text{SG}} = 0.7(3)$  and  $\gamma_{\text{SG}} = 1.7(5)$ . One sees that these exponents are not far from the mean-field exponents expected above the upper critical dimension  $D = 6$ .

In the SK case, mean-field exponents should be exact. Indeed, as shown in Fig.9, our data of  $q_s^{(2)}$  are entirely consistent with such a mean-field behavior,  $\beta_{\text{SG}} = 1$  and  $\eta_{\text{SG}} = 0$ <sup>25,26</sup>.

In concluding this section, we touch upon the near-critical behavior of the spin observed around the chiral-glass transition point in 4D. Although our data of the Binder ratios and the overlap distribution functions given above have strongly suggested that the Heisenberg spin remains paramagnetic even below  $T_{\text{CG}}$  in 4D, the present  $q_s^{(2)}$  data can be scaled reasonably well with assuming  $T_{\text{SG}}/J = T_{\text{CG}}/J = 0.38(2)$ , at least from the purely numerical viewpoint. Such a constrained finite-size scaling analysis of  $q_s^{(2)}$  yields the estimates  $\nu'_{\text{SG}} = 1.3(2)$  and  $\eta'_{\text{SG}} = -0.7(2)$ : See Fig.10 (a). Note that the value of  $\nu'$  is far from the LCD value,  $\nu' = \infty$ . We also note that the same  $q_s^{(2)}$  data can also be fitted with a comparable quality by assuming a zero-temperature SG transition,  $T_{\text{SG}} = 0$ : See Fig.10 (b). As mentioned, we believe that the  $\nu'_{\text{SG}}$  and  $\eta'_{\text{SG}}$  values obtained by assuming  $T_{\text{SG}} = T_{\text{CG}}$  do not represent true asymptotic exponent values, but just represent *effective exponents describing the short-scale near-critical phenomena which is an echo of the chiral-glass transition*. Indeed, at short scales, the chirality is never independent of the spin by its definition. Hence, the behavior of the spin-correlation related quantities might well reflect the critical singularity associated with the *chirality* up to certain length and time scales.

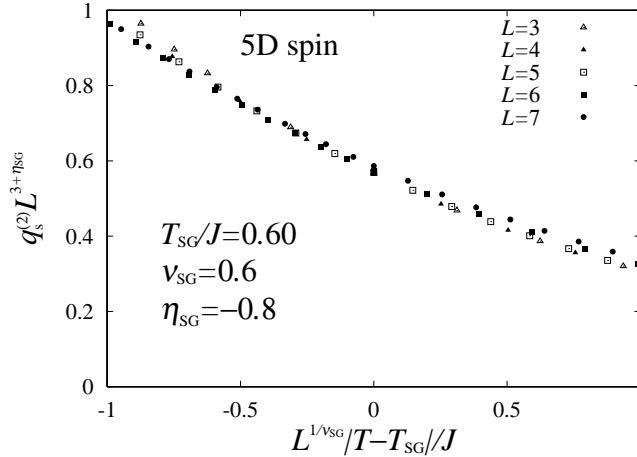


FIG. 8: Finite-size scaling plot of the spin-glass order parameter in 5D.

## V. SUMMARY AND DISCUSSION

In summary, we performed a large-scale equilibrium MC simulation of the 4D, 5D and SK Heisenberg spin glasses. In 5D, the model exhibits a single SG transition at a finite temperature, reminiscent to the one of the corresponding mean-field model. Below the transition temperature  $T_{\text{SG}}/J = 0.60(2)$ , the spin is frozen in a spatially random noncoplanar configuration. Although the SG order accompanies a finite chiral-glass LRO reflecting the noncoplanar nature of the spin order, the order parameter of the transition is the spin, not the chirality, and the chiral-glass susceptibility remains nondiverging at  $T = T_{\text{SG}}$ . Similar behavior is also observed in the Heisenberg SK model. The SG exponents in 5D are estimated as  $\alpha = -1.0(5)$ ,  $\beta_{\text{SG}} = 0.7(3)$ ,  $\gamma_{\text{SG}} = 1.7(5)$  and  $\nu_{\text{SG}} = 0.6(2)$ , most of which are rather close to the mean-field exponents. Since the upper critical dimension of the SG is believed to be

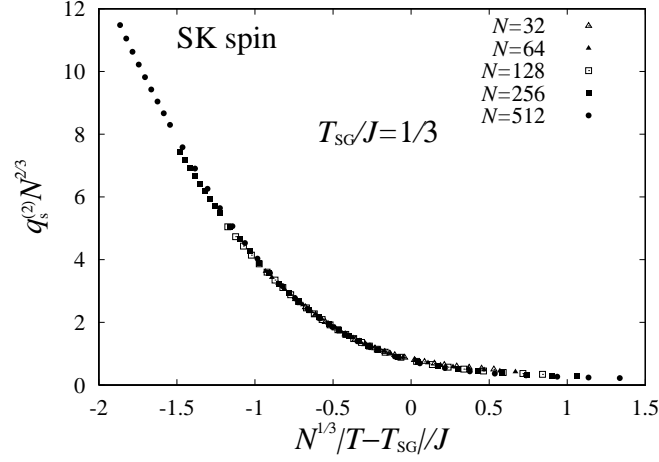


FIG. 9: Finite-size scaling plot of the spin-glass order parameter in the SK model.

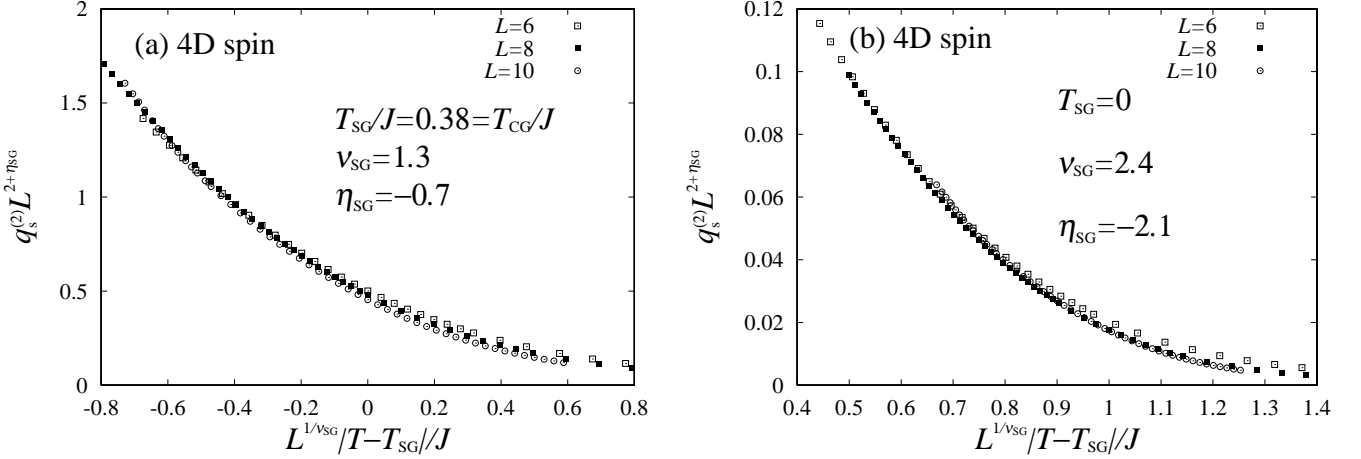


FIG. 10: Finite-size scaling plot of the spin-glass order parameter in 4D, assuming (a)  $T_{SG}/J = T_{CG}/J = 0.38$  and (b)  $T_{SG} = 0$ . In (b), our best value of  $\eta_{SG}$  is reasonably close to the exact value of  $\eta_{SG} = -2$  expected for the  $T = 0$  transition.

six, the observed closeness to the mean-field values seems reasonable. Our data suggest that the SG ordered state accompanies a peculiar phase-space structure, namely, a one-step-like RSB, at least in its chiral sector. Such a one-step-like character of the RSB is at variance with the full (hierarchical) RSB realized in the SK model corresponding to  $D = \infty$ . It means that the RSB pattern of the ordered state changes its nature at some borderline dimensionality, presumably at the upper critical dimension  $D = 6$ .

In 4D, the model exhibits a significantly different behavior from the 5D and the SK models. Bulk of our data, particularly the Binder ratio, indicate that the 4D model exhibits a pure chiral-glass transition at a finite temperature  $T_{CG} = 0.38(2)$  without accompanying the standard SG order. At the chiral-glass transition, however, the spin becomes almost critical which manifests itself as a pseudo-critical phenomenon observable at short length scales. The critical region associated with the chiral-glass transition is very narrow, limited to  $t \lesssim 10^{-2}$ , suggesting that the dimension four is close to the marginal dimensionality. The SG transition occurs either at  $T_{SG} = 0$  or at a finite temperature, but below the chiral-glass transition temperature,  $T_{SG} < T_{CG}$ . Our data suggest that the chiral-glass ordered state accompanies a one-step-like RSB in the chiral sector. Again, such a one-step-like character of the RSB differs from the full (hierarchical) RSB realized in the SK model.

Next, we wish to compare our present results on the 4D and 5D Heisenberg SGs with those of the previous authors. To our knowledge, our results for the chiral order are new. Concerning the spin order, our present conclusion, *i.e.*,

the presence of the SG LRO in 5D and the absence of it in 4D, is consistent with most of numerical simulations, in particular, with the one of Stauffer and Binder<sup>19</sup>. Our conclusion, however, is at variance with that of Coluzzi, who suggested that the SG LRO set in at a finite temperature  $T_{\text{SG}}/J \simeq 0.5$ <sup>20</sup>. Although the numerical data themselves seem to be consistent between the two works, Coluzzi simulated rather small lattices  $L \leq 5$  and high temperatures  $T/J \geq 0.5$ , which hampered a direct examination of the asymptotic ordering behavior. Our new data for larger lattices  $L \leq 10$  and for temperatures including lower ones,  $T/J \geq 0.26$ , have clarified that the transition occurs in the chiral sector at  $T_{\text{CG}}/J \simeq 0.4$ , which is somewhat lower than  $T_{\text{SG}}$  estimated in Ref.<sup>20</sup>. Furthermore, the Heisenberg spin appears to remain paramagnetic at the chiral-glass transition point on sufficiently long length scales, *i.e.*, the transition at  $T_{\text{CG}}/J \simeq 0.4$  is *not* the conventional SG transition, but a pure chiral-glass transition.

Finally, we wish to discuss implication of our present result to the 3D case. The behavior of the 4D model observed in the present work is qualitatively similar to the one of the 3D model observed in Refs.<sup>10,15</sup>, except that the behavior of the 4D model looks much more marginal. For example, the reduced chiral-glass susceptibility of the 3D model is much larger in magnitude than that of the 4D model, and the associated chiral-glass critical region is much wider in 3D than in 4D. As one judges from the size dependence of the reduced chiral-glass susceptibility shown in Fig.3 of Ref.<sup>10</sup>, the width of the chiral critical region is about  $10^{-1}$ , which should be compared with our present estimate for the 4D model,  $10^{-2}$ . All these suggest that the spin-chirality decoupling is more eminent in lower dimensions. As the dimensionality is increased, the spin-chirality decoupling tends to be suppressed. In 4D, the spin-chirality decoupling still seems to persist, but it is limited only to a very narrow temperature region close to the transition temperature, suggesting that 4D is close to the borderline dimensionality. As the dimensionality is further increased, the spin-chirality decoupling no longer occurs. There, the order parameter of transition is the spin, not the chirality. This is indeed the case for 5D. However, at least in the case of 5D, the SG ordered state exhibits a peculiar one-step-like RSB, which differs in character from the full RSB of the  $D = \infty$  SK model. Estimated SG critical exponents of the 5D model are rather close to the mean-field values, which is consistent with a common belief that the mean-field SG exponents arise above six dimensions.

### Acknowledgements

The numerical calculation was performed on the HITACHI SR8000 at the supercomputer system, ISSP, University of Tokyo, and Intel Pentium4 1.8GHz PCs in our laboratory. The authors are thankful to Dr. K. Hukushima and Dr. H. Yoshino for useful discussion.

### APPENDIX A: DERIVATION OF EQ.(7)

In this appendix, we give the derivation of Eq.(7). It describes the self-overlap part of the diagonal spin-overlap distribution function in the thermodynamic limit, when the SG ordered state with a nonzero EA order parameter  $q_s^{\text{EA}} > 0$  exists. Since the diagonal spin-overlap  $q_{\text{diag}}$  transforms nontrivially under global  $O(3)$  rotations, even a self-overlap part of the distribution function is not just a simple delta function located at  $q_{\text{diag}} = \pm q_s^{\text{EA}}$ , but exhibits a nontrivial behavior given by Eq.(7).

We consider a diagonal spin-overlap between a particular spin state described by the configuration  $\vec{S}_i$  and a state generated from this state via a global  $O(3)$  rotation  $R$ ,

$$q_{\text{diag}} = \frac{1}{N} \sum_{i=1}^N \vec{S}_i \cdot R \vec{S}_i \quad . \quad (\text{A1})$$

We first consider the case of proper rotations with  $\det(R)=1$ . The  $SO(3)$  rotation matrix  $R$  is known to be parametrized by the Euler angles,  $\Phi$ ,  $\Theta$  and  $\Psi$ , as

$$R = \begin{pmatrix} R_{xx} & R_{xy} & R_{xz} \\ R_{yx} & R_{yy} & R_{yz} \\ R_{zx} & R_{zy} & R_{zz} \end{pmatrix} = \begin{pmatrix} \cos \Theta \cos \Phi \cos \Psi - \sin \Phi \sin \Psi & \cos \Theta \sin \Phi \cos \Psi + \sin \Phi \cos \Psi & -\sin \Theta \cos \Psi \\ -\cos \Theta \cos \Phi \sin \Psi - \sin \Phi \cos \Psi & -\cos \Theta \sin \Phi \sin \Psi + \cos \Phi \cos \Psi & \sin \Theta \sin \Psi \\ \sin \Theta \cos \Phi & \sin \Theta \sin \Phi & \cos \Theta \end{pmatrix} \quad .$$

Then,  $q_{\text{diag}}$  can be written as

$$q_{\text{diag}} = \frac{1}{N} \sum_{i=1}^N (R_{xx} S_{ix}^2 + R_{yy} S_{iy}^2 + R_{zz} S_{iz}^2 + (R_{xy} + R_{yx}) S_{ix} S_{iy} + (R_{yz} + R_{zy}) S_{iy} S_{iz} + (R_{zx} + R_{xz}) S_{iz} S_{ix}) \quad . \quad (\text{A2})$$

The spin direction at each site can be represented as  $\vec{S}_i = (\sin \theta_i \cos \phi_i, \sin \theta_i \sin \phi_i, \cos \phi_i)$ . If one notes the fact that, in the SG ordered state, the spin direction is entirely random on long length scales giving a uniform distribution on a sphere in spin space, one can replace in the thermodynamic limit the summation over spins by the integral over spin directions as  $(1/N) \sum_{i=1}^N \rightarrow (1/4\pi) \int_{-1}^1 d\cos \theta \int_0^{2\pi} d\phi$ . Then, only the diagonal terms containing  $R_{\mu\mu}$  survive in Eq.(A2), leading to

$$q_{\text{diag}} = \frac{\cos(\Phi + \Psi) + 1}{3} \cos \Theta + \frac{\cos(\Phi + \Psi)}{3} = \frac{\cos(\Phi + \Psi) + 1}{3} x + \frac{\cos(\Phi + \Psi)}{3} , \quad (\text{A3})$$

where  $x \equiv \cos \Theta$ . Note that this is a function of the rotation matrix  $R$  only, not depending on the spin configuration  $\vec{S}_i$  any more. The overlap  $q_{\text{diag}}$  takes various values depending on the  $O(3)$  matrix  $R$ . We then consider the distribution of  $q_{\text{diag}}$  arising from the distribution of  $R$ , or equivalently,  $x$ ,  $\Phi$  and  $\Psi$ . The appropriate measure is  $-1 \leq x \leq 1$ ,  $0 \leq \Phi < 2\pi$  and  $0 \leq \Psi < 2\pi$  being uniform. It is convenient to change the variables from  $(\Phi, \Psi)$  to  $(\alpha, \beta) = (\Phi + \Psi, (-\Phi + \Psi)/2)$ , where  $0 \leq \alpha < 4\pi$  and  $0 \leq \beta < \pi$ . With this change of the variables, Eq.(A3) becomes independent of  $\beta$ , and is given by

$$q_{\text{diag}} = \frac{\cos \alpha + 1}{3} x + \frac{\cos \alpha}{3} . \quad (\text{A4})$$

The distribution function  $P_s(q_{\text{diag}})$  is proportional to

$$\begin{aligned} P_s(q_{\text{diag}}) &\propto \int \frac{dx}{dq_{\text{diag}}} d\alpha \\ &= \int_0^{\alpha_c(q_{\text{diag}})} \frac{3}{1 + \cos \alpha} d\alpha , \end{aligned} \quad (\text{A5})$$

where we have used Eq.(A3). Note that, for a given  $q_{\text{diag}}$ , the integral with respect to  $\alpha$  is restricted to the range  $[0, \alpha_c]$ , with  $\alpha_c(q_{\text{diag}}) = \cos^{-1}[(3q_{\text{diag}} - 1)/2]$ . This may be seen from Fig.11, where we plot  $q_{\text{diag}}$  as a function of  $x$  for various  $\alpha$ . Obviously, for a given  $q_{\text{diag}}$ , no contribution to the integral arises from the region of  $\alpha$  between  $[\alpha_c, \pi]$ . The  $q_{\text{diag}}$ -dependence of  $P_s(q_{\text{diag}})$  arises from this upper limit of the integral. The integration in Eq.(A5) can be easily

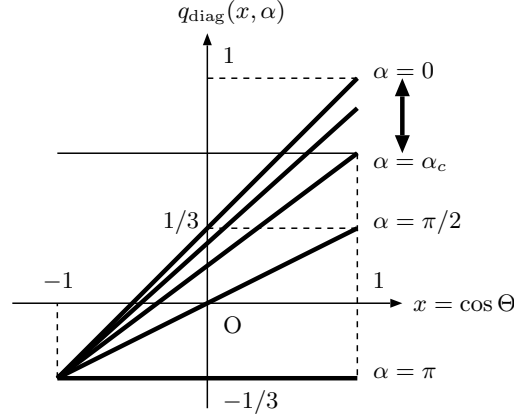


FIG. 11: Sketch of  $q_{\text{diag}}$  as a function of  $x$  for various  $\alpha$ . For a given value of  $q_{\text{diag}}$ , there is no possible value of  $x$  for a range of  $\alpha$  satisfying  $\alpha_c(q_{\text{diag}}) \leq \alpha \leq \pi$ .

carried out to yield,

$$P_s(q_{\text{diag}}) \propto \tan \frac{\alpha_c(q_{\text{diag}})}{2} = 3^{1/2} \sqrt{\frac{1 - q_{\text{diag}}}{3q_{\text{diag}} + 1}} .$$

So far, we have considered proper rotations. The contribution from improper rotations, which can be viewed as proper rotations combined with the spin inversion  $\vec{S}_i \rightarrow -\vec{S}_i$ , may be obtained immediately by the replacement  $q_{\text{diag}} \rightarrow$



$-q_{\text{diag}}$ . Adding the contributions from both proper and improper rotations with equal weights, and reproducing the appropriate normalization factor, we get

$$P_s(q_{\text{diag}}) = \frac{3\sqrt{3}}{4\pi} \left( \sqrt{\frac{1 - q_{\text{diag}}}{3q_{\text{diag}} + 1}} + \sqrt{\frac{1 + q_{\text{diag}}}{-3q_{\text{diag}} + 1}} \right). \quad (\text{A6})$$

Finally, we note that at finite temperatures a state should be regarded as a pure state. The spin length is then no longer unity, and the unity in Eq.(A6) should be replaced by  $q_s^{\text{EA}}$ . We finally obtain

$$P_s(q_{\text{diag}}) = \frac{3\sqrt{3}}{4\pi q_s^{\text{EA}}} \left( \sqrt{\frac{q_s^{\text{EA}} - q_{\text{diag}}}{3q_{\text{diag}} + q_s^{\text{EA}}}} + \sqrt{\frac{q_s^{\text{EA}} + q_{\text{diag}}}{-3q_{\text{diag}} + q_s^{\text{EA}}}} \right), \quad (\text{A7})$$

which is Eq.(7).

The derivation above, valid in the thermodynamic limit  $N \rightarrow \infty$ , is quite general. In order to get some feeling about the finite-size effect, we also compute  $P_s(q_{\text{diag}})$  numerically for finite- $N$  Heisenberg spins, the direction of which is assumed to be completely random in three-component spin space. More specifically, we prepare a random and uncorrelated configuration of  $N$  spins, numerically generate  $O(3)$  rotation matrix  $R$  with appropriate measure (*i.e.*, the one generated randomly from the uniform distribution of  $-1 \leq x \leq 1$ ,  $0 \leq \Phi < 2\pi$ ,  $0 \leq \Psi < 2\pi$  and the determinant  $\pm 1$ ), operate  $R$  to the initial spin configuration, and compute the diagonal spin-overlap  $q_{\text{diag}}$  between the initial and the  $O(3)$ -rotated spin configurations. We generate  $10^4$  distinct  $O(3)$  matrices for a given initial spin configuration, and generate several hundreds of initial spin configurations,  $P_s(q_{\text{diag}})$  being accumulated over these procedures. The result is shown in Fig.12. The  $N = \infty$  result analytically obtained above is also shown. It can be seen that the rounded peak at  $\pm \frac{1}{3}q_s^{\text{EA}}$  grows as  $N$  increases, eventually exhibiting a divergent behavior in the  $N = \infty$  limit. Of course, the finite- $N$  result computed here is valid only for non-interacting spins. It would differ from the corresponding result for the interacting system, in contrast to the analytical  $N = \infty$  result which is valid even for the interacting system. It still gives some feeling how the finite-size rounding takes place in finite- $N$  SG models.

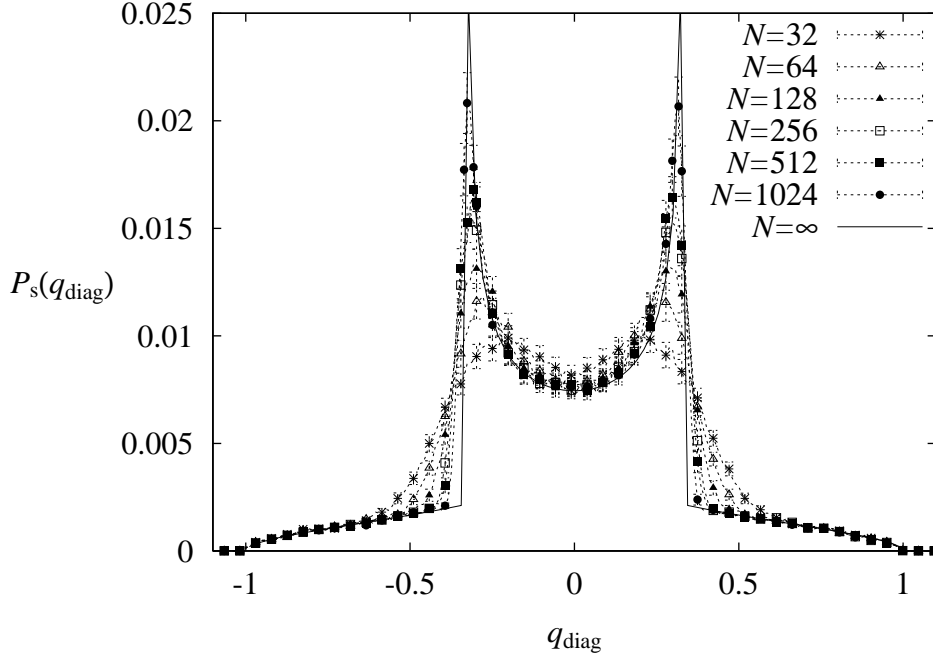


FIG. 12: The diagonal spin-overlap distribution function  $P_s(q_{\text{diag}})$  of finite-size systems of  $N$  Heisenberg spins with completely random, uncorrelated spin configurations. The result for  $N = \infty$  given by Eq.(7) is also shown by the solid curve. For further details, see the text.

---

\* Electronic address: imag@spin.ess.sci.osaka-u.ac.jp

- <sup>†</sup> Electronic address: kawamura@ess.sci.osaka-u.ac.jp; URL: <http://thmat8.ess.sci.osaka-u.ac.jp/~kawamura>
- <sup>1</sup> For reviews on spin glasses, see *e. g.*, K. Binder and A. P. Young: Rev. Mod. Phys. **58** 801 (1986); K. H. Fischer and J. A. Hertz: *Spin Glasses* (Cambridge University Press, Cambridge, 1991); J. A. Mydosh: *Spin Glasses*, (Taylor & Francis, London-Washington DC, 1993); *Spin glasses and random fields*, ed. A. P. Young (World Scientific, Singapore, 1997).
- <sup>2</sup> J. A. Olive, A. P. Young and D. Sherrington, Phys. Rev. B **34**, 6341 (1986).
- <sup>3</sup> J. R. Banavar and M. Cieplak, Phys. Rev. Lett. **48**, 832 (1982).
- <sup>4</sup> W. L. McMillan, Phys. Rev. B **31**, 342 (1985).
- <sup>5</sup> F. Matsubara, T. Iyota and S. Inawashiro, Phys. Rev. Lett. **67**, 1458 (1991).
- <sup>6</sup> H. Kawamura, Phys. Rev. Lett. **68** 3785 (1992); Int. J. Mod. Phys. C **7**, 6341 (1996).
- <sup>7</sup> H. Yoshino and H. Takayama, Europhys. Lett. **22**, 631 (1993).
- <sup>8</sup> H. Kawamura, J. Phys. Soc. Jpn. **64**, 26 (1995).
- <sup>9</sup> H. Kawamura, Phys. Rev. Lett. **80**, 5421 (1998).
- <sup>10</sup> K. Hukushima and H. Kawamura, Phys. Rev. E **61**, R1008 (2000).
- <sup>11</sup> H. Kawamura and D. Imagawa, Phys. Rev. Lett. **87**, 207203 (2001).
- <sup>12</sup> D. Imagawa and H. Kawamura, J. Phys. Soc. Jpn. **71**, 127 (2002).
- <sup>13</sup> F. Matsubara, S. Endoh and T. Shirakura, J. Phys. Soc. Jpn. **69**, 1927 (2000); S. Endoh, F. Matsubara and T. Shirakura, J. Phys. Soc. Jpn. **70** 1543 (2001); F. Matsubara, T. Shirakura and S. Endoh, Phys. Rev. B **64**, 092412 (2001).
- <sup>14</sup> T. Nakamura and S. Endoh, J. Phys. Soc. Jpn. **71**, 2113 (2002).
- <sup>15</sup> K. Hukushima and H. Kawamura, unpublished.
- <sup>16</sup> P. Reed: J. Phys. C **11**, L979 (1978).
- <sup>17</sup> M. Cieplak and J. R. Banavar, Phys. Rev. B **29**, 469 (1984).
- <sup>18</sup> P. W. Anderson and C. MorganPond, Phys. Rev. Lett. **40**, 903 (1978).
- <sup>19</sup> D. Stauffer and K. Binder, Z. Phys. B **41**, 237 (1981).
- <sup>20</sup> B. Coluzzi, J. Phys. A Math. Gen **28**, 747 (1995).
- <sup>21</sup> K. Hukushima and K. Nemoto, J. Phys. Soc. Jpn. **65**, 1604 (1995).
- <sup>22</sup> H. G. Katzgraber, M. Palassini and A. P. Young, Phys. Rev. B **63**, 184422 (2001).
- <sup>23</sup> H. G. Katzgraber and A. P. Young, Phys. Rev. B **65**, 214401 (2002).
- <sup>24</sup> H. Kawamura and M. S. Li, Phys. Rev. Lett. **87**, 187204 (2001).
- <sup>25</sup> R. Botet, R. Jullien and P. Pfeuty, Phys. Rev. Lett. **49**, 478 (1982).
- <sup>26</sup> K. Hukushima and H. Kawamura, Phys. Rev. E **62**, 3360 (2000).